Interplay of Surface and Interior Modes in Exciton-Phonon Coupling at the Nanoscale

Dipti Jasrasaria*,† and Eran Rabani*,†,‡,¶

†*Department of Chemistry, University of California, Berkeley, California 94720, United States*

‡*The Sackler Center for Computational Molecular and Materials Science, Tel Aviv University, Tel Aviv, Israel 69978*

¶*Materials Sciences Division, Lawrence Berkeley National Laboratory, Berkeley, California 94720, United States*

E-mail: djasrasaria@berkeley.edu; eran.rabani@berkeley.edu

Abstract

Exciton-phonon coupling (EXPC) plays a key role in the optoelectronic properties of semiconductor nanocrystals (NCs). Despite its importance, a microscopic picture of EXPC is still lacking, particularly regarding the magnitude and scaling with NC size, the dependence on phonon frequency, and the role of the NC surface. Due to the computational complexity associated with accurately describing excitons and phonons, previous theoretical studies of EXPC have been limited to small NCs, noninteracting electron-hole models, and/or a small number of phonon modes. Here, we develop an atomistic approach for describing EXPC in NCs of experimentally relevant sizes. We validate our approach by calculating reorganization energies, a measure of EXPC, for a series of CdSe and CdSe-CdS core-shell NCs, finding good agreement with experimental measurements. We demonstrate that exciton formation distorts the NC lattice primarily along the coordinates of low-frequency acoustic modes that are delocalized over the entire NC. Modes at the NC surface play a significant role in smaller NCs while coupling to interior modes dominates for larger systems.

Keywords

exciton-phonon coupling, reorganization energy, semiconductor nanocrystals, quantum dots, nanocrystal surfaces

Semiconductor nanocrystals (NCs) are promising for a variety of applications due to their highly tunable optoelectronic properties. Many of these technologies, such as solar cells,[1–3] lasers,[4] and bioimaging probes,[5] rely on electronic excited states. Understanding the non-radiative decay and dephasing of these excited states, which are dictated by the exciton-phonon coupling (EXPC) in these systems, is key to the rational design of NC-based technologies with reduced thermal losses and increased quantum yields. A framework for calculating accurate EXPC in NCs is essential for modeling observables like homogenous linewidths[6,7] and processes like phonon-mediated hot carrier cooling[8–11] and charge transfer.[12]

In bulk semiconductors, lower-frequency acoustic modes, which involve in-phase movements of atoms, couple to electronic degrees of freedom via the deformation potential, which

describes how strain and deformation of the crystal lattice change the excitonic energies.[13] In polar crystals, like CdSe and other II-VI materials, the piezoelectric potential also couples electrons and acoustic phonons, although its effect is much weaker.[13,14] Optical phonons are higher in frequency and consist of out-of-phase motions of atoms. They couple to the electronic degrees of freedom through the Fröhlich mechanism, or the interaction between the dipole polarization field generated by optical phonons and the excitonic charge density.[13] While excitons and phonons are expected to interact via similar mechanisms in confined semiconductor NCs, the effects of quantum confinement and the resulting magnitudes of EXPC are still not well understood.

Quantum confinement in NCs leads to the discretization of excitonic states with energy gaps that vary and can be much larger than the typical phonon frequencies. Therefore, higher-frequency optical phonons may be more relevant than acoustic phonons in dynamical processes, such as exciton dephasing or relaxation, that occur via phonon absorption or emission, regardless of the magnitude of their coupling to excitons. Similarly, motion at the NC surface may be important to exciton dynamics, even if phonon modes localized near the surface are weakly coupled to excitons.[15–17]

Experimentally, these dynamical effects as well as those of structural NC defects often confound measurements of the EXPC and have thus led to conflicting results. Some observations indicate stronger EXPC to acoustic modes,[18–21] and others show stronger EXPC to optical modes.[22–26] From a theoretical perspective,[14,27–37] progress has been limited due to the computational complexity associated with accurately describing excitons and phonons, to which the magnitude of the resulting EXPC is extremely sensitive,[22] in NC systems of experimentally relevant sizes. These challenges have led to a set of outstanding questions regarding EXPC in semiconductor NCs: the relative coupling strengths of excitons to acoustic versus optical modes, the scaling of EXPC with system size, and the role of the NC surface in EXPC.

In this Letter, we introduce an atomistic approach that provides a framework to address these questions and bridges our understanding of EXPC in molecular and bulk systems to provide fundamental insight into EXPC at the nanoscale. We focus on the intrinsic EXPC and compute reorganization energies for wurtzite CdSe NCs with diameters ranging from ∼2–5 nm as well as CdSe-CdS core-shell NCs to obtain a systematic understanding of the EXPC and its dependence on NC size, phonon frequency, and phonon localization (surface versus interior). The reorganization energies we calculate for CdSe NCs correspond well to those obtained experimentally by absorption and photoluminescence measurements. Our results demonstrate that core-shell NCs have smaller reorganization energies than bare CdSe NCs, but EXPC to acoustic modes that are delocalized across the NC contribute more significantly to the reorganization energy in all NC systems. Excitons in smaller NCs are more strongly coupled to modes localized near the surface of the NC, while excitons in larger NCs are more strongly coupled to modes in the interior of the NC.

We begin by stating the standard Hamiltonian that describes a manifold of excitonic states and phonons that are coupled to first order in the atomic displacements:[38]

$$H = \sum_n E_n \left|\psi_n\right\rangle \left\langle\psi_n\right| + \sum_\alpha \hbar\omega_\alpha b_\alpha^\dagger b_\alpha + \sum_{\alpha nm} V_{n,m}^\alpha \left|\psi_n\right\rangle \left\langle\psi_m\right| q_\alpha \,, \tag{1}$$

where $|\psi_n\rangle$ is the wavefunction of exciton n with energy E_n, and $b_\alpha^\dagger$ and b_α are the Boson creation and annihilation operators, respectively, of phonon mode α with frequency ω_α and coordinate $q_\alpha = \sqrt{\frac{\hbar}{2\omega_\alpha}}\left(b_\alpha^\dagger + b_\alpha\right)$. Note that the crystal momentum does not appear in this Hamiltonian due to the lack of translational symmetry in NC systems.

To obtain accurate descriptions of both the excitons and phonons in Eq. (1), we develop an atomistic approach that is computationally feasible for NC systems of experimentally relevant sizes. The excitonic states $|\psi_n\rangle$ and their

corresponding energies E_n in the first term of Eq. (1) were obtained from atomistic electronic structure calculations within the semi-empirical pseudopotential method.[39–41] To compute the quasiparticle (i.e. electron and hole) states near the conduction and valence band edges, respectively, we used the filter-diagonalization technique[41] with the single-particle Hamiltonian taken at the equilibrium configuration of the nanocrystal,

$$h = -\frac{1}{2}\nabla_{\boldsymbol{r}}^2 + \sum_{\mu} v_{\mu}\left(|\boldsymbol{r} - \boldsymbol{R}_{0,\mu}|\right) , \qquad (2)$$

where $v_{\mu}\left(|\boldsymbol{r} - \boldsymbol{R}_{0,\mu}|\right)$ is the effective pseudopotential for atom μ with equilibrium position $\boldsymbol{R}_{0,\mu}$. Excitonic (i.e. correlated electron-hole pair) states are written as linear combinations of product electron-hole states,

$$\psi_n\left(\boldsymbol{r}_e, \boldsymbol{r}_h\right) = \sum_{ai} c_{a,i}^n \phi_a\left(\boldsymbol{r}_e\right) \phi_i\left(\boldsymbol{r}_h\right) , \qquad (3)$$

where the coefficients $c_{a,i}^n$ are determined by solving the Bethe-Salpeter equation.[42] In the above equation, $\phi_a\left(\boldsymbol{r}_e\right)$ is the wavefunction of an electron in orbital a, and $\phi_i\left(\boldsymbol{r}_h\right)$ is the wavefunction of a hole in orbital i. This approach has been shown to predict quantitatively accurate excitonic properties, such as absorption and emission spectra[43] and Auger recombination lifetimes.[42]

The phonon modes and frequencies in the second term of Eq. (1) were modeled using previously parametrized Stillinger-Weber interaction potentials.[44] The dynamical matrix, or mass-weighted Hessian, was computed at the equilibrium configuration:[45,46]

$$D_{\mu k,\mu' k'} = \frac{1}{\sqrt{m_{\mu} m_{\mu'}}} \left(\frac{\partial^2 U\left(\boldsymbol{R}\right)}{\partial u_{\mu k} \partial u_{\mu' k'}} \right)_{\boldsymbol{R}_0} , \qquad (4)$$

where $U\left(\boldsymbol{R}\right)$ is the Stillinger-Weber potential energy of the surface, $u_{\mu k} = R_{\mu k} - R_{0,\mu k}$ is the displacement of nucleus μ away from its equilibrium position in the $k \in \{x, y, z\}$ direction, and m_{μ} is the mass of nucleus μ. The normal modes and corresponding frequencies were then obtained by diagonalizing this $3N \times 3N$ dynamical matrix, where N is the number of atoms in the NC.

The coupling between excitonic states and phonons to lowest order in the phonon mode coordinate is described by the third term of Eq. (1). Within our electronic structure model, the standard electron-phonon matrix element[38,47] is equal to

$$\begin{aligned} V_{n,m}^{\mu k} &\equiv \left\langle \psi_n \left| \left(\frac{\partial v_{\mu}\left(|\boldsymbol{r} - \boldsymbol{R}_{\mu}|\right)}{\partial R_{\mu k}} \right)_{\boldsymbol{R}_0} \right| \psi_m \right\rangle \\ &= \sum_{abi} c_{a,i}^n c_{b,i}^m v'_{ab,\mu}\left(R_{\mu k}\right) \\ &\quad - \sum_{aij} c_{a,i}^n c_{a,j}^m v'_{ij,\mu}\left(R_{\mu k}\right) , \end{aligned} \qquad (5)$$

where

$$v'_{rs,\mu}\left(R_{\mu k}\right) = \int d\boldsymbol{r} \phi_r\left(\boldsymbol{r}\right) \frac{\partial v_{\mu}\left(|\boldsymbol{r} - \boldsymbol{R}_{\mu}|\right)}{\partial R_{\mu k}} \phi_s\left(\boldsymbol{r}\right) . \qquad (6)$$

Here, $v_{\mu}\left(|\boldsymbol{r} - \boldsymbol{R}_{\mu}|\right)$ is the atomic pseudopotential introduced in Eq. (2), $\phi_s\left(\boldsymbol{r}\right)$ is the wavefunction of a single-particle electron state ($s \in a, b$) or hole state ($s \in i, j$), and $c_{a,i}^n$ are the coefficients introduced in Eq. (3) that are obtained from solving the Bethe-Salpeter equation. See the Supporting Information for a detailed derivation of the matrix elements in Eq. (5).

Note that the EXPC matrix element can be split into two terms, as written in the last line of Eq. (5). The first term describes the electron channel, which couples excitons comprised of different single-particle electron states but the same hole state, and the second term describes the hole channel, which couples excitons comprised of different hole states but the same electron state. These selection rules result from the fact that the EXPC is a matrix element of a one-body operator ($\partial v / \partial R$). However, we emphasize that all calculations performed in this work are within an interacting framework of correlated electron-hole states, as illustrated in the first line of Eq. (5).

The matrix elements in Eq. (5) are computed directly and then transformed to phonon mode coordinates to obtain the EXPC matrix ele-

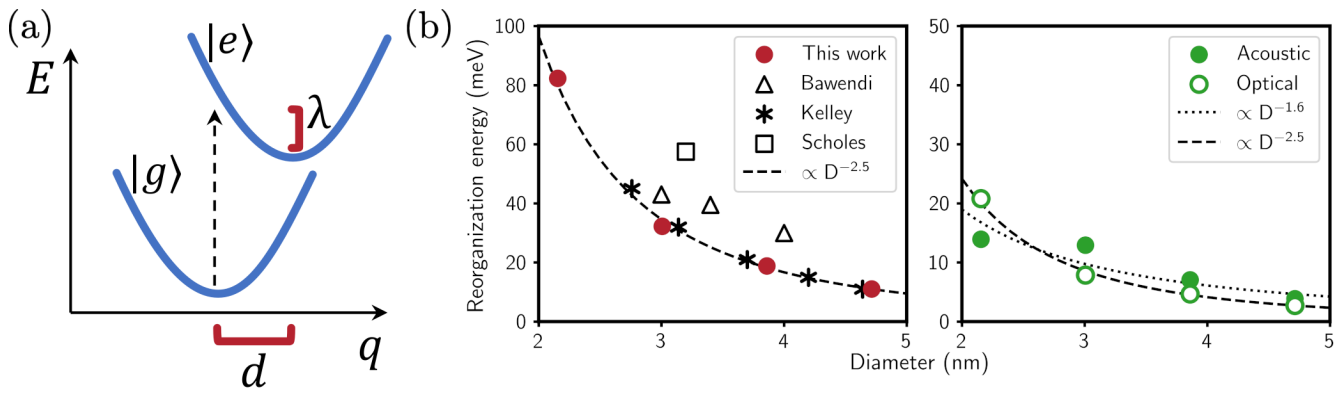

Figure 1: (a) The reorganization energy λ corresponds to the energy associated with the rearrangement of the lattice after a vertical excitation from the ground state $|g\rangle$ to the excited state $|e\rangle$. The minima of the ground and excited states are displaced by a distance d along the phonon mode coordinate q. (b) Reorganization energies computed in this work for CdSe NCs of various diameters in comparison to values from effective mass model-based calculations by Kelley[31] and from experimental measurements by Bawendi et al.[48] and Scholes et al.[18] (left). Acoustic modes contribute more significantly to the reorganization energy than optical modes (right).

ments in the third term of Eq. (1):

$$V^{\alpha}_{n,m} = \sum_{\mu k} \frac{1}{\sqrt{m_\mu}} e^{-1}_{\alpha,\mu k} V^{\mu k}_{n,m}\,, \tag{7}$$

where $e_{\alpha,\mu k}$ is the μk element of the α eigenvector of the dynamical matrix.

The matrix elements $V^{\alpha}_{n,n}$ describe how the energy of excitonic state $|\psi_n\rangle$ is renormalized through its interaction with phonon mode α, and the matrix elements $V^{\alpha}_{n,m}$ describe how excitonic states $|\psi_n\rangle$ and $|\psi_m\rangle$ are coupled through the absorption or emission of a phonon of mode α.

We validate our model through the computation of the reorganization energy for a series of CdSe NCs. As illustrated schematically in Figure 1a, the reorganization energy λ is the energy associated with the rearrangement of the NC lattice after a vertical electronic excitation (i.e. Condon approximation). In the harmonic approximation, the total reorganization energy for a NC is the sum of the reorganization energies for each mode, $\lambda = \sum_\alpha \lambda_\alpha$, where

$$\lambda_\alpha = \frac{1}{Z}\sum_n e^{-\beta E_n} \frac{1}{2}\left(\frac{1}{\omega_\alpha} V^{\alpha}_{n,n}\right)^2 . \tag{8}$$

Eq. (8) includes a Boltzmann-weighted average over excitonic states $|\psi_n\rangle$, where $Z = \sum_n e^{-\beta E_n}$ is the partition function, and $\beta = 1/k_B T$, where T is the temperature. All excitonic states included in the average at room temperature (T = 298 K) have contributions mainly from the LUMO and from several hole states near the HOMO, consistent with the heavier effective mass of the hole and the larger density of hole states.

The reorganization energies for wurtzite CdSe cores with diameters of 2.2 nm, 3.0 nm, 3.9 nm, and 4.7 nm were calculated to be between 90 and 30 meV (Figure 1b), which compare favorably with values obtained from a parameterized effective mass model[31] and from room-temperature absorption and photoluminescence measurements of the Stokes shift,[18,48] which is assumed to be equal to twice the reorganization energy.[18,49] The reorganization energy decreases with increasing NC diameter D, with a scaling that roughly follows a power law: $\propto D^{-1.4}$. Excitons with smaller coherence areas are more sensitive to their local environment, explaining that EXPC is stronger in smaller NCs. Higher-energy excitonic states tend to be more delocalized and thus have smaller reorganization energies,[20,31] as calculated for these systems and illustrated in Figure S1.

To better understand the scaling of the reorganization energy with system size, we ex-

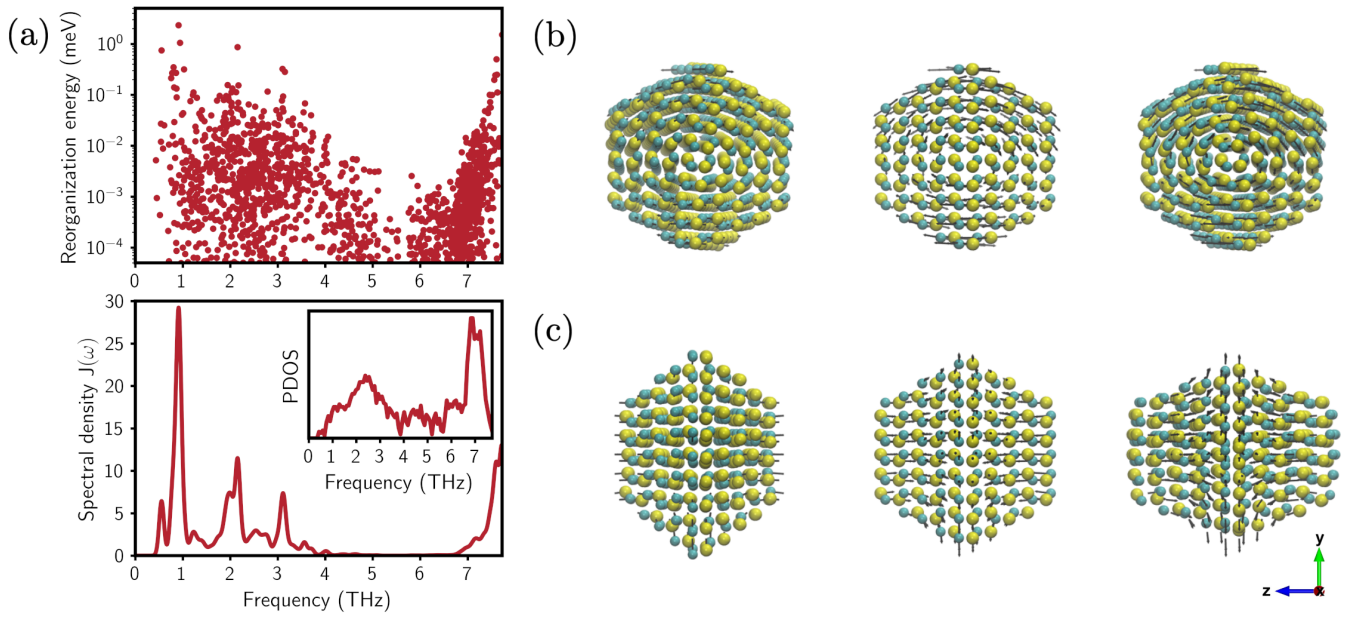

Figure 2: (a) The reorganization energies per mode (top), spectral density (bottom), and phonon density of states (inset) calculated for a 3.9 nm CdSe NC. The circle and triangle in the top panel correspond to the modes depicted in Figures 2b and 2c, respectively. (b) Torsional mode with a frequency of 0.45 THz and reorganization energy of 1.20 meV. (c) Breathing mode with a frequency of 0.55 THz and reorganization energy of 1.03 meV.

amine contributions to the total reorganization energy from acoustic modes ($\omega < 1$ THz) and optical modes ($\omega > 4$ THz), as shown in Figure 1b, where the frequency cut-offs were determined from the CdSe bulk phonon dispersion relation.[50] Modes at intermediate frequencies ($1 < \omega < 4$ THz) are difficult to characterize due to overlap of the acoustic and optical branches in the bulk phonon dispersion relation and the confounding effect of phonon confinement.[50] For strongly confined NCs, like the ones studied here with $D < 5$ nm, we find that lower-frequency acoustic modes contribute more significantly to the reorganization energy than higher-frequency optical modes. Additionally, the reorganization energies of lower-frequency modes scale more steeply with system size as $\lambda_{\mathrm{ac}} \propto D^{-1.7}$ than those of optical modes, which scale as $\lambda_{\mathrm{op}} \propto D^{-1.4}$. These scaling dependencies match those expected from simple continuum models,[14,22] which predict $\lambda_{\mathrm{ac}} \propto D^{-2}$ and $\lambda_{\mathrm{op}} \propto D^{-1}$, as shown in the Supporting Information.

To determine the contributions of specific modes, we analyzed the reorganization energy for each mode for a 3.9 nm CdSe NC, the results of which are plotted in Figure 2a. Modes with frequencies lower than 1.5 THz contribute most significantly, and two modes in particular have large reorganization energies of 1.202 meV and 1.033 meV. These modes are depicted in Figures 2b and 2c and are animated in Supporting Videos S1 and S2.[51,52] They are the torsional and breathing (spheroidal) acoustic modes that are delocalized throughout the NC and involve collective motions of many atoms.

While these results indicate that lower-frequency acoustic modes are more strongly coupled to the exciton, the optical phonons may be important in dynamical processes despite their relatively weaker coupling. This significance may be due to a higher density of phonon states at those optical frequencies (Figure 2a inset), which are more relevant given the energy scales of typical excitonic transitions. This interplay can be further investigated through the weighted phonon density of states, or spectral density,

$$J(\omega) = \sum_{\alpha} \lambda_{\alpha} \delta(\omega - \omega_{\alpha}) \,, \tag{9}$$

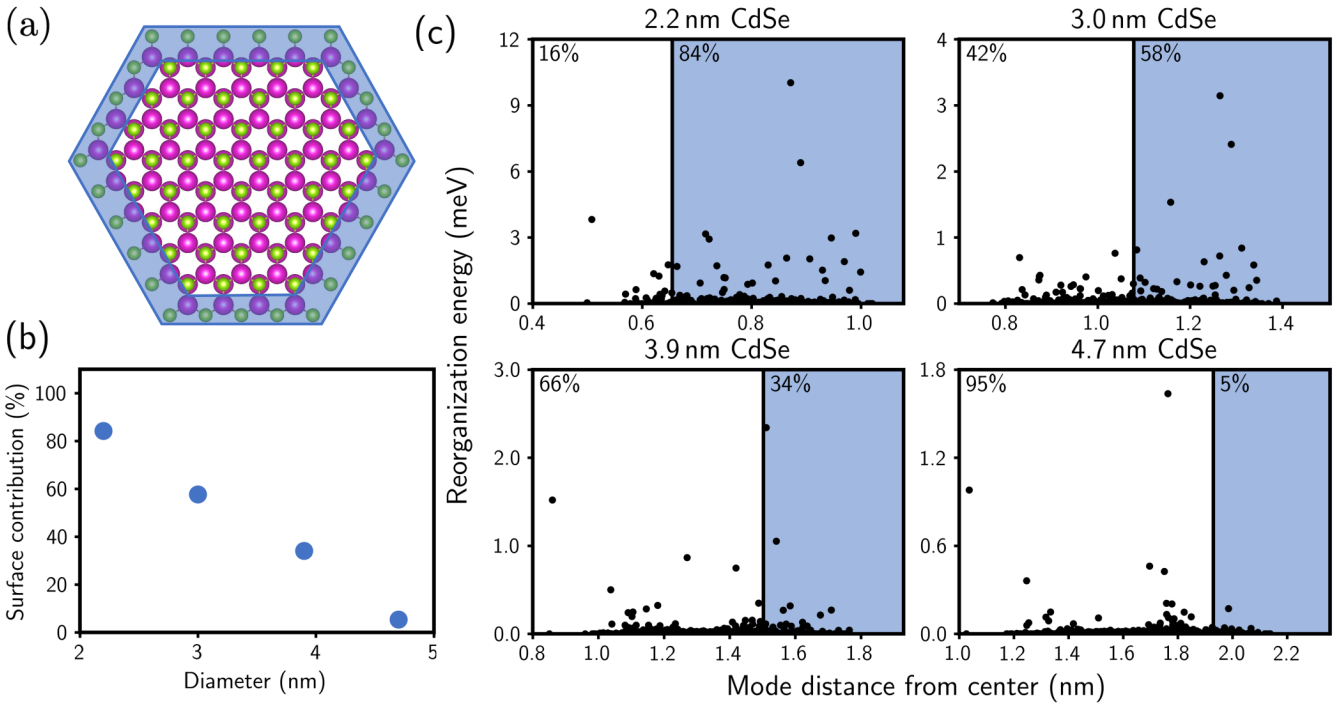

Figure 3: (a) Cross-section of a 3.9 nm CdSe NC with the outer ML shaded in blue. (b) The contribution to the total reorganization energy from modes localized to the surface decreases with increasing NC size. (c) The reorganization energy with phonon mode distance from the NC center for a series of CdSe NCs. Modes in the blue shaded regions are localized to the NC surface. The circle and triangle in the bottom left panel indicate the torsional and breathing modes illustrated in Figures 2b and 2c, respectively. The numbers in the top left of each panel correspond to the percent contributions of the interior (white) and surface (blue) modes to the total reorganization energy.

which is plotted in Figure 2a for the same 3.9 nm CdSe NC. The Dirac delta functions in Eq. (9) were broadened as Gaussian functions with a standard deviation of 0.05 THz, and they are normalized such that $\lambda = \int d\omega J(\omega)$. The spectral density peaks at 0.832 THz (3.44 meV) and decays at higher frequencies. However, the spectral density shows another peak at 6.84 THz (28.3 meV) in the range of the longitudinal optical phonon, which has been predicted and shown to play a role in phonon-mediated exciton relaxation and dephasing.[6,7,53] Our calculations show that exciton formation distorts the NC lattice primarily along coordinates of low-frequency torsional and spheroidal phonon modes, but non-negligible EXPC to optical modes, in addition to the large density of phonon states at those higher frequencies, support their role in exciton dynamics.

Another question regarding EXPC in nanostructures is the effect of phonon confinement and whether phonon modes localized near the NC surface are inherently more strongly coupled to excitons than modes localized to the interior of the NC. To investigate these surface effects, we define the distance of phonon mode α from the center of the NC as

$$r_\alpha \equiv \sum_{\mu k} e^2_{\alpha,\mu k} r_\mu \,, \tag{10}$$

where r_μ is the distance of atom μ from the center of the NC. Note that phonon modes comprised primarily of motion from surface atoms have a large value of r_α, and they can be delocalized over the NC. Figure S2 and Supporting Videos S3 and S4 show two different phonon modes of a 3.9 nm CdSe NC; the first corresponds to a mode with a large value of r_α, and the second corresponds to a mode with a small value of r_α.

Figure 3a depicts a cross-section of a 3.9 nm CdSe NC with the outermost monolayer (ML)

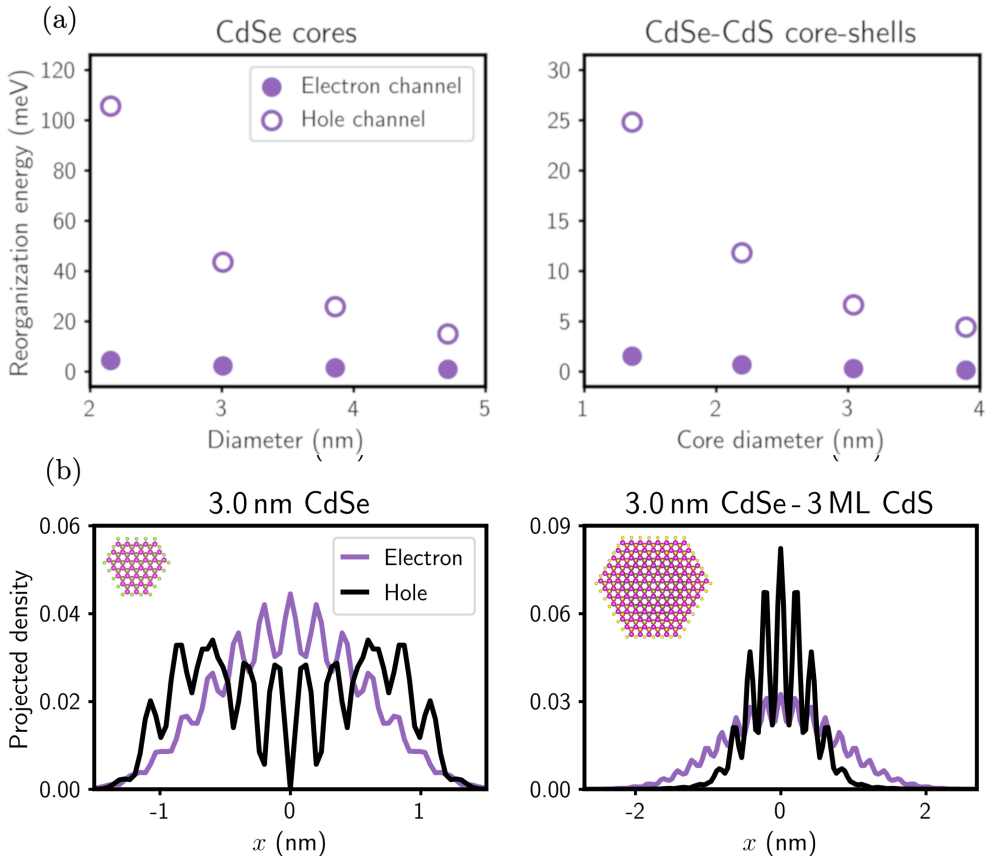

Figure 4: (a) Reorganization energies for CdSe (left) and CdSe-CdS core-shell (right) NCs of various sizes divided into contributions from the electron and hole channels. Reorganization energies for the core-shell NCs are an order of magnitude smaller than those of bare CdSe NCs. (b) Hole and electron carrier densities of the lowest-energy excitonic state for a 3.0 nm CdSe NC (left) and 3.0 nm CdSe – 3 ML CdS NC (right).

of atoms highlighted in blue. The reorganization energy of each mode as a function of the mode distance from the NC center is illustrated in Figure 3c. For the smallest NC with a diameter of 2.2 nm, phonon modes localized to the outer ML have a total reorganization energy of 88 meV, which is 99% of the total reorganization energy. For this system, 92% of the modes are localized to the outer ML because of the relatively large surface area to volume ratio for a NC of such small size. The EXPC to these modes is relatively strong, as the exciton extends to the surface of the NC due to the large quantum confinement.

The contribution to the reorganization energy from surface modes decreases with increasing NC diameter (Figure 3b). This trend is a result of the decreasing surface area to volume ratio as well as the decreasing quantum confinement in larger NCs, which leads to localization of the exciton wavefunction near the center of the NC and reduces the EXPC to surface modes. For a 4.7 nm CdSe NC, the interplay between surface and interior modes favors the interior modes, which contribute 24 meV or 78% of the total reorganization energy. EXPC of interior modes with larger r_α values is greater than that of interior modes localized to the center of the NC. But, the total number of interior modes increases linearly with NC size and dominates contributions to the reorganization energy for large NCs.

The increased EXPC to surface modes in smaller NCs may explain photoluminescence measurements that observe broadened and red-shifted emission, which is attributed to emission from NC surface states, that increases with decreasing NC size.[7,54,55] Larger coupling of the exciton to surface modes in smaller NCs may facilitate phonon-mediated exciton trapping to

surface states, thereby increasing photoluminescence from the surface.

The large contribution of surface modes to the reorganization energy of small NCs suggests that treatment of the NC surface, such as in core-shell NCs, could be used to control the magnitude of EXPC. As seen in Figure 4a, the reorganization energy for CdSe cores with 3 MLs of CdS shell is about an order of magnitude smaller than for bare cores of the same size. These values, ranging from approximately 10 meV to 2 meV for CdSe core sizes ranging from 1.4 nm to 3.9 nm, agree with optical measurements of the Stokes shift.[56]

This dramatic reduction is due to suppression of the hole channel of the EXPC (second term in the last line of Eq. (5)), which contributes more significantly to the reorganization energy (Figure 4a). The quasi-type II band alignment of CdSe-CdS core-shell structures confines the exciton hole to the core, as illustrated in Figure 4b. This hole confinement limits EXPC to modes that are delocalized over the NC. Because these low-frequency, delocalized modes generally have larger EXPC than higher-frequency, localized modes, the overall reorganization energy is decreased in core-shell NCs.

For both core and core-shell systems, the hole channel of the EXPC is more significant than the electron channel because of the heavier hole effective mass, which makes the hole states more sensitive to the nuclear configuration, as well as the smaller energy spacing between hole states, which allows them to couple more readily via phonon absorption or emission.

Investigation of the reorganization energy with mode distance from the center for each core-shell NC (Figure 5) shows that, despite the confinement of the hole to the core, modes localized to the core have a negligible contribution to the total reorganization energy. In the smallest core-shell system, a 1.4 nm CdSe – 3 ML CdS NC, many modes are localized to the NC surface and comprise 44% of the reorganization energy. For larger core-shell systems, however, fewer modes are at the surface, and modes with r_α values that correspond to the NC shell have the most significant contributions to the reorganization energy. These shell modes tend to be delocalized and consist of motion from both atoms near the surface and throughout the core. These results clearly indicate that, while the overall magnitude of EXPC is dictated by the relative localization of the carriers, EXPC is always strongest to those phonon modes that are delocalized across the NC and involve collective motion from many atoms in the system.

In conclusion, the approach outlined in this Letter provides a framework for computing EXPC in NCs that reproduces experimental results. Furthermore, our ability to calculate the EXPC to each phonon mode provides the first microscopic, atomistic approach of EXPC with frequency that reconciles discrepancies in previous observations regarding the relative magnitude of EXPC to acoustic versus optical phonons. We demonstrate that exciton formation distorts the NC lattice along phonon coordinates of low-frequency acoustic modes due to the inherently stronger coupling of excitons to these modes relative to that of excitons to optical modes. However, we also show that optical modes may be important in phonon-mediated exciton dynamics due to the large phonon density of states at those frequencies, which are at an energy scale that is more relevant for excitonic transitions. We also provide insight into the role of phonon confinement and the NC surface. Our results indicate that in small systems with diameters less than 4 nm, where the number of surface modes is large and the exciton wavefunction is strongly quantum confined and extends to the NC surface, modes localized to the outer ML of the NC dominate contributions to the reorganization energy. However, the surface contribution decreases linearly with increasing system size. For all systems, even core-shell systems in which the exciton hole is confined to the core, EXPC is strongest to modes that are delocalized throughout the NC.

These calculations provide valuable insight into EXPC at the nanoscale. Furthermore, the framework presented here is general and can be applied to study anisotropic NCs, like nanorods and nanoplatelets, to understand the role of dimensionality on EXPC, and to study III-V materials, such as InAs and InP, which have gained

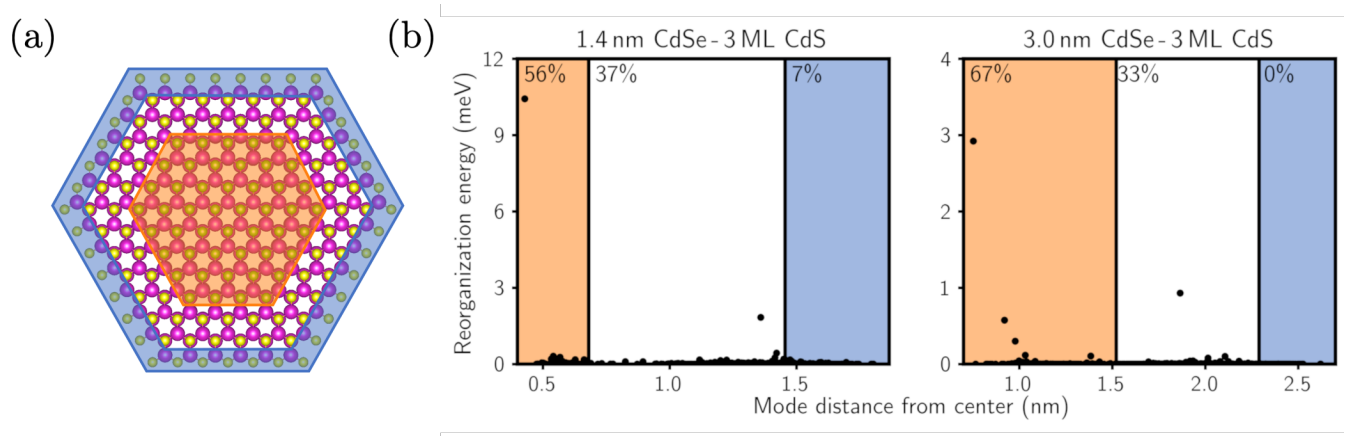

Figure 5: (a) Cross-section of a 3.0 nm CdSe – 3 ML CdS NC with the core shaded in orange and the outer ML shaded in blue. (b) The reorganization energy with phonon mode distance from the NC center for two CdSe-CdS core-shell NCs. Modes in the orange and blue shaded regions are localized to the NC core and surface, respectively. The numbers in the top left of each panel correspond to the percent contributions of the core (orange), shell (white), and surface (blue) modes to the total reorganization energy.

interest due to their near-infrared emission. Finally, an accurate description of EXPC enables future work for understanding the timescales and mechanisms of phonon-mediated exciton dynamics, like hot carrier cooling, exciton dephasing, and charge transport, which is essential in promoting the rational design of NCs with quantum yields necessary for the realization of new technologies.

Supporting Information Available

Procedure used to construct nanocrystal configurations, additional discussion regarding the implementation of the semi-empirical pseudopotential method, filter-diagonalization technique, and Bethe-Salpeter equation, derivation of exciton-phonon coupling matrix elements, scaling of reorganization energies for acoustic and optical phonon modes, reorganization energies for higher-energy excitonic states, and illustrations and animations of surface and interior phonon modes.

Acknowledgement The authors thank Daniel Weinberg for help with pseudopotential fitting. E.R. acknowledges support from the Department of Energy, Photonics at thermodynamic Limits Energy Frontier Research Center, under Grant No. DESC0019140. Methods used in this work were provided by the Center for Computational Study of Excited State Phenomena in Energy Materials (C2SEPEM), which is funded by the U.S. Department of Energy, Office of Science, Basic Energy Sciences, Materials Sciences and Engineering Division, via Contract No. DE-AC02-05CH11231, as part of the Computational Materials Sciences Program. D.J. acknowledges the support of the Computational Science Graduate Fellowship from the U.S. Department of Energy under Grant No. DE-SC0019323.

References

(1) Klimov, V. I. Spectral and Dynamical Properties of Multiexcitons in Semiconductor Nanocrystals. *Annu. Rev. Phys. Chem.* **2007**, *58*, 635–673.

(2) Bronstein, N. D.; Yao, Y.; Xu, L.; O'Brien, E.; Powers, A. S.; Ferry, V. E.; Alivisatos, A. P.; Nuzzo, R. G. Quantum Dot Luminescent Concentrator Cavity Exhibiting 30-fold Concentration. *ACS Photonics* **2015**, *2*, 1576–1583.

(3) Xu, J. et al. 2D Matrix Engineering for Homogeneous Quantum Dot Coupling

in Photovoltaic Solids. *Nat. Nanotechnol.* **2018**, *13*, 456–462.

(4) Ledentsov, N. N. Quantum Dot Laser. *Semicond. Sci. Technol.* **2011**, *26*, 1–8.

(5) Kairdolf, B. A.; Smith, A. M.; Stokes, T. H.; Wang, M. D.; Young, A. N.; Nie, S. Semiconductor Quantum Dots for Bioimaging and Biodiagnostic Applications. *Annu. Rev. Anal. Chem.* **2013**, *6*, 143–162.

(6) Cui, J. et al. Evolution of the Single-Nanocrystal Photoluminescence Linewidth with Size and Shell: Implications for Exciton-Phonon Coupling and the Optimization of Spectral Linewidths. *Nano Lett.* **2016**, *16*, 289–296.

(7) Mack, T. G.; Jethi, L.; Kambhampati, P. Temperature Dependence of Emission Line Widths from Semiconductor Nanocrystals Reveals Vibronic Contributions to Line Broadening Processes. *J. Phys. Chem. C* **2017**, *121*, 28537–28545.

(8) Nozik, A. J. Spectroscopy and Hot Electron Relaxation Dynamics in Semiconductor Quantum Wells and Quantum Dots. *Annu. Rev. Phys. Chem.* **2001**, 193–231.

(9) Kilina, S. V.; Kilin, D. S.; Prezhdo, O. V. Breaking the Phonon Bottleneck in PbSe and CdSe Quantum Dots: Time-Domain Density Functional Theory of Charge Carrier Relaxation. *ACS Nano* **2009**, *3*, 93–99.

(10) Kambhampati, P. Unraveling the Structure and Dynamics of Excitons in Semiconductor Quantum Dots. *Acc. Chem. Res.* **2011**, *44*, 1–13.

(11) Kambhampati, P. Hot Exciton Relaxation Dynamics in Semiconductor Quantum Dots: Radiationless Transitions on the Nanoscale. *J. Phys. Chem. C* **2011**, *115*, 22089–22109.

(12) Tvrdy, K.; Frantsuzov, P. A.; Kamat, P. V. Photoinduced Electron Transfer from Semiconductor Quantum Dots to Metal Oxide Nanoparticles. *Proc. Natl. Acad. Sci. U. S. A.* **2011**, *108*, 29–34.

(13) Mahan, G. D. *Many-Particle Physics*; 2000.

(14) Takagahara, T. Electron-Phonon Interactions in Semiconductor Nanocrystals. *J. Lumin.* **1996**, *70*, 129–143.

(15) Bozyigit, D.; Yazdani, N.; Yarema, M.; Yarema, O.; Lin, W. M. M.; Volk, S.; Vuttivorakulchai, K.; Luisier, M.; Juranyi, F.; Wood, V. Soft Surfaces of Nanomaterials Enable Strong Phonon Interactions. *Nature* **2016**, *531*, 618–622.

(16) Mack, T. G.; Jethi, L.; Andrews, M.; Kambhampati, P. Direct Observation of Vibronic Coupling between Excitonic States of CdSe Nanocrystals and Their Passivating Ligands. *J. Phys. Chem. C* **2019**, *123*, 5084–5091.

(17) Guzelturk, B. et al. Dynamic Lattice Distortions Driven by Surface Trapping in Semiconductor Nanocrystals. *Nat. Commun.* **2021**, *12*, 1–9.

(18) Salvador, M. R.; Graham, M. W.; Scholes, G. D. Exciton-Phonon Coupling and Disorder in the Excited States of CdSe Colloidal Quantum Dots. *J. Chem. Phys.* **2006**, *125*, 184709.

(19) Morello, G.; De Giorgi, M.; Kudera, S.; Manna, L.; Cingolani, R.; Anni, M. Temperature and Size Dependence of Nonradiative Relaxation and Exciton-Phonon Coupling in Colloidal CdTe Quantum Dots. *J. Phys. Chem. C* **2007**, *111*, 5846–5849.

(20) Sagar, D. M.; Cooney, R. R.; Sewall, S. L.; Dias, E. A.; Barsan, M. M.; Butler, I. S.; Kambhampati, P. Size Dependent, State-Resolved Studies of Exciton-Phonon Couplings in Strongly Confined Semiconductor Quantum Dots. *Phys. Rev. B: Con-*

dens. Matter Mater. Phys. **2008**, *77*, 1–14.

(21) Sagar, D. M.; Cooney, R. R.; Sewall, S. L.; Kambhampati, P. State-Resolved Exciton-Phonon Couplings in CdSe Semiconductor Quantum Dots. *J. Phys. Chem. C* **2008**, *112*, 9124–9127.

(22) Nomura, S.; Kobayashi, T. Exciton–LO-Phonon Couplings in Spherical Semiconductor Microcrystallites. *Phys. Rev. B: Condens. Matter Mater. Phys.* **1992**, *45*, 1305.

(23) Scamarcio, G.; Spagnolo, V.; Ventruti, G.; Lugará, M.; Righini, G. Size Dependence of Electron–LO-Phonon Coupling in Semiconductor Nanocrystals. *Phys. Rev. B: Condens. Matter Mater. Phys.* **1996**, *53*, R10489–R10492.

(24) Heitz, R.; Mukhametzhanov, I.; Stier, O.; Madhukar, A.; Bimberg, D. Enhanced Polar Exciton-LO-Phonon Interaction in Quantum Dots. *Phys. Rev. Lett.* **1999**, *83*, 4654–4657.

(25) Lin, C.; Gong, K.; Kelley, D. F.; Kelley, A. M. Electron-Phonon Coupling in CdSe/CdS Core/Shell Quantum Dots. *ACS Nano* **2015**, *9*, 8131–8141.

(26) Lin, C.; Gong, K.; Kelley, D. F.; Kelley, A. M. Size-Dependent Exciton-Phonon Coupling in CdSe Nanocrystals through Resonance Raman Excitation Profile Analysis. *J. Phys. Chem. C* **2015**,

(27) Klein, M. C.; Hache, F.; Ricard, D.; Flytzanis, C. Size Dependence of Electron-Phonon Coupling in Semiconductor Nanospheres: The Case of CdSe. *Phys. Rev. B: Condens. Matter Mater. Phys.* **1990**, *42*, 11123–11132.

(28) Marini, J. C.; Stebe, B.; Kartheuser, E. Exciton-Phonon Interaction in CdSe and CuCl Polar Semiconductor Nanospheres. *Phys. Rev. B: Condens. Matter Mater. Phys.* **1994**, *50*, 14302–14308.

(29) Hamma, M.; Miranda, R. P.; Vasilevskiy, M. I.; Zorkani, I. Calculation of the Huang-Rhys Parameter in Spherical Quantum Dots: The Optical Deformation Potential Effect. *J. Phys. Condens. Matter* **2007**, *19*, 1–12.

(30) Chu, I. H.; Radulaski, M.; Vukmirovic, N.; Cheng, H. P.; Wang, L. W. Charge Transport in a Quantum Dot Supercrystal. *J. Phys. Chem. C* **2011**, *115*, 21409–21415.

(31) Kelley, A. M. Electron-Phonon Coupling in CdSe Nanocrystals from an Atomistic Phonon Model. *ACS Nano* **2011**, *5*, 5254–5262.

(32) Han, P.; Bester, G. First-Principles Calculation of the Electron-Phonon Interaction in Semiconductor Nanoclusters. *Phys. Rev. B: Condens. Matter Mater. Phys.* **2012**, *85*, 1–7.

(33) Yazdani, N.; Bozyigit, D.; Vuttivorakulchai, K.; Luisier, M.; Infante, I.; Wood, V. Tuning Electron-Phonon Interactions in Nanocrystals through Surface Termination. *Nano Lett.* **2018**, *18*, 2233–2242.

(34) Han, P.; Bester, G. Fundamental Difference Between Measured and Calculated Exciton-Phonon Coupling in Nanostructures. *Phys. Rev. B: Condens. Matter Mater. Phys.* **2019**, *99*, 1–6.

(35) Yazdani, N.; Andermatt, S.; Yarema, M.; Farto, V.; Bani-Hashemian, M. H.; Volk, S.; Lin, W. M.; Yarema, O.; Luisier, M.; Wood, V. Charge Transport in Semiconductors Assembled from Nanocrystal Quantum Dots. *Nat. Commun.* **2020**, *11*, 1–9.

(36) Yazdani, N.; Volk, S.; Yarema, O.; Yarema, M.; Wood, V. Size, Ligand, and Defect-Dependent Electron-Phonon Coupling in Chalcogenide and Perovskite Nanocrystals and Its Impact on Luminescence Line Widths. *ACS Photonics* **2020**, *7*, 1088–1095.

(37) Zeng, T.; He, Y. Ab initio Modeling of Phonon-Assisted Relaxation of Electrons and Excitons in Semiconductor Nanocrystals for Multiexciton Generation. *Phys. Rev. B: Condens. Matter Mater. Phys.* **2021**, *103*, 1–15.

(38) Giustino, F. Electron-Phonon Interactions from First Principles. *Rev. Mod. Phys.* **2017**, *89*, 1–63.

(39) Wang, L. W.; Zunger, A. Electronic Structure Pseudopotential Calculations of Large (Approximately 1000 Atoms) Si Quantum Dots. *J. Phys. Chem.* **1994**, *98*, 2158–2165.

(40) Wang, L. W.; Zunger, A. Pseudopotential Calculations of Nanoscale CdSe Quantum Dots. *Phys. Rev. B: Condens. Matter Mater. Phys.* **1996**, *53*, 9579–9582.

(41) Rabani, E.; Hetényi, B.; Berne, B. J.; Brus, L. E. Electronic Properties of CdSe Nanocrystals in the Absence and Presence of a Dielectric Medium. *J. Chem. Phys.* **1999**, *110*, 5355–5369.

(42) Philbin, J. P.; Rabani, E. Electron-Hole Correlations Govern Auger Recombination in Nanostructures. *Nano Lett.* **2018**, *18*, 7889–7895.

(43) Hadar, I.; Philbin, J. P.; Panfil, Y. E.; Neyshtadt, S.; Lieberman, I.; Eshet, H.; Lazar, S.; Rabani, E.; Banin, U. Semiconductor Seeded Nanorods with Graded Composition Exhibiting High Quantum-Yield, High Polarization, and Minimal Blinking. *Nano Lett.* **2017**, *17*, 2524–2531.

(44) Zhou, X. W.; Ward, D. K.; Martin, J. E.; Van Swol, F. B.; Cruz-Campa, J. L.; Zubia, D. Stillinger-Weber Potential for the II-VI Elements Zn-Cd-Hg-S-Se-Te. *Phys. Rev. B: Condens. Matter Mater. Phys.* **2013**, *88*, 1–14.

(45) Plimpton, S. Fast Parallel Algorithms for Short-Range Molecular Dynamics. *J. Comput. Phys.* **1995**, *117*, 1–19.

(46) Kong, L. T. Phonon Dispersion Measured Directly from Molecular Dynamics Simulations. *Comput. Phys. Commun.* **2011**, *182*, 2201–2207.

(47) Grimvall, G. *The Electron-Phonon Interaction in Metals*; 1981.

(48) Liptay, T. J.; Marshall, L. F.; Rao, P. S.; Ram, R. J.; Bawendi, M. G. Anomalous Stokes Shift in CdSe Nanocrystals. *Phys. Rev. B: Condens. Matter Mater. Phys.* **2007**, *76*, 1–7.

(49) Ekimov, A. I.; Hache, F.; Schanne-Klein, M. C.; Ricard, D.; Flytzanis, C.; Kudryavtsev, I. A.; Yazeva, T. V.; Rodina, A. V.; Efros, A. L. Absorption and Intensity-Independent Photoluminescence Measurements on CdSe Quantum Dots: Assignment of the First Electronic Transitions. *J. Opt. Soc. Am. B* **1993**, *10*, 100–107.

(50) Grünwald, M.; Zayak, A.; Neaton, J. B.; Geissler, P. L.; Rabani, E. Transferable Pair Potentials for CdS and ZnS Crystals. *J. Chem. Phys.* **2012**, *136*, 234111.

(51) Bakan, A.; Meireles, L. M.; Bahar, I. ProDy: Protein Dynamics Inferred from Theory and Experiments. *Bioinf.* **2011**, *27*, 1575–1577.

(52) Bakan, A.; Dutta, A.; Mao, W.; Liu, Y.; Chennubhotla, C.; Lezon, T. R.; Bahar, I. Evol and ProDy for Bridging Protein Sequence Evolution and Structural Dynamics. *Bioinf.* **2014**, *30*, 2681–2683.

(53) Palato, S.; Seiler, H.; Nijjar, P.; Prezhdo, O.; Kambhampati, P. Atomic Fluctuations in Electronic Materials Revealed by Dephasing. *Proc. Natl. Acad. Sci. U. S. A.* **2020**, *117*, 0–6.

(54) Mooney, J.; Krause, M. M.; Saari, J. I.; Kambhampati, P. A Microscopic Picture of Surface Charge Trapping in Semiconductor Nanocrystals. *J. Chem. Phys.* **2013**, *138*, 204705.

(55) Jethi, L.; Mack, T. G.; Kambhampati, P. Extending Semiconductor Nanocrystals from the Quantum Dot Regime to the Molecular Cluster Regime. *J. Phys. Chem. C* **2017**, *121*, 26102–26107.

(56) Talapin, D. V.; Koeppe, R.; Götzinger, S.; Kornowski, A.; Lupton, J. M.; Rogach, A. L.; Benson, O.; Feldmann, J.; Weller, H. Highly Emissive Colloidal CdSe/CdS Heterostructures of Mixed Dimensionality. *Nano Lett.* **2003**, *3*, 1677–1681.

TOC Graphic

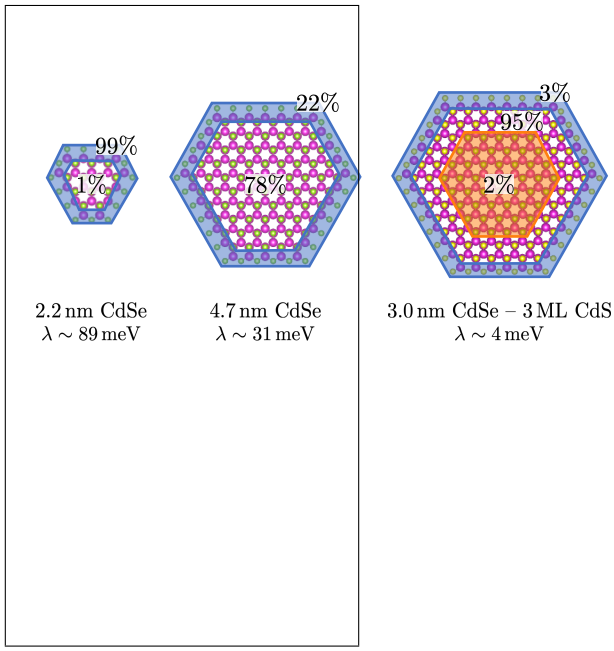
99%
1%
22%
78%
3%
95%
2%
2.2 nm CdSe
λ ∼ 89 meV
4.7 nm CdSe
λ ∼ 31 meV
3.0 nm CdSe – 3 ML CdS
λ ∼ 4 meV

Correction to "Interplay of Surface and Interior Modes in Exciton-Phonon Coupling at the Nanoscale"

Dipti Jasrasaria*,† and Eran Rabani*,†,‡,¶

†*Department of Chemistry, University of California, Berkeley, California 94720, United States*

‡*The Sackler Center for Computational Molecular and Materials Science, Tel Aviv University, Tel Aviv, Israel 69978*

¶*Materials Sciences Division, Lawrence Berkeley National Laboratory, Berkeley, California 94720, United States*

E-mail: djasrasaria@berkeley.edu; eran.rabani@berkeley.edu

Nano Lett. **2021**, *21 (20)* 8741–8748. DOI: 10.1021/acs.nanolett.1c02953

We identified a small error in the code used to perform the calculations of exciton-phonon couplings presented in this work. The corrected code results in small quantitative differences and minor qualitative differences, as reflected in the corrected figures below. The corrected results show that the reorganization energies of higher-frequency, optical modes scales as $\lambda_{\text{op}} \propto D^{-2.5}$. Additionally, in core-shell NCs, phonon modes localized to the core of the NC dominate contributions to the reorganization energy. All equations presented in the original paper are correct. This correction does not influence the discussions or conclusions of the original paper.

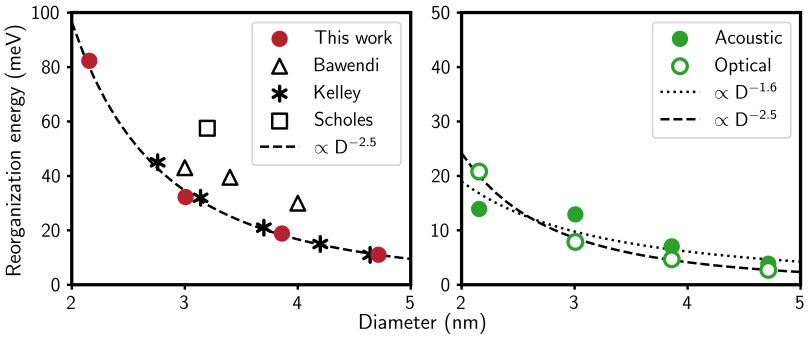

Figure 1: (b) Reorganization energies computed in this work for CdSe NCs of various diameters in comparison to values from effective mass model-based calculations by Kelley [1] and from experimental measurements by Bawendi et al. [2] and Scholes et al. [3] (left). Acoustic modes contribute more significantly to the reorganization energy than optical modes (right).

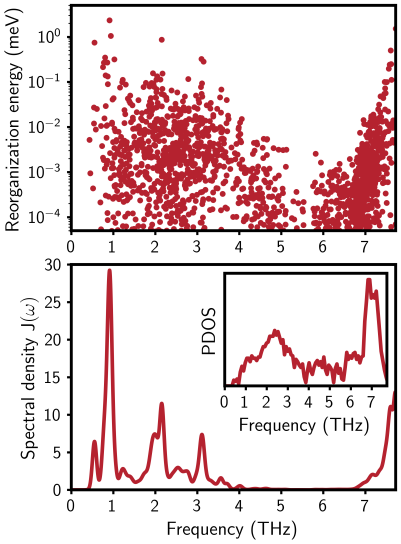

Figure 2: (a) The reorganization energies per mode (top), spectral density (bottom), and phonon density of states (inset) calculated for a 3.9 nm CdSe NC.

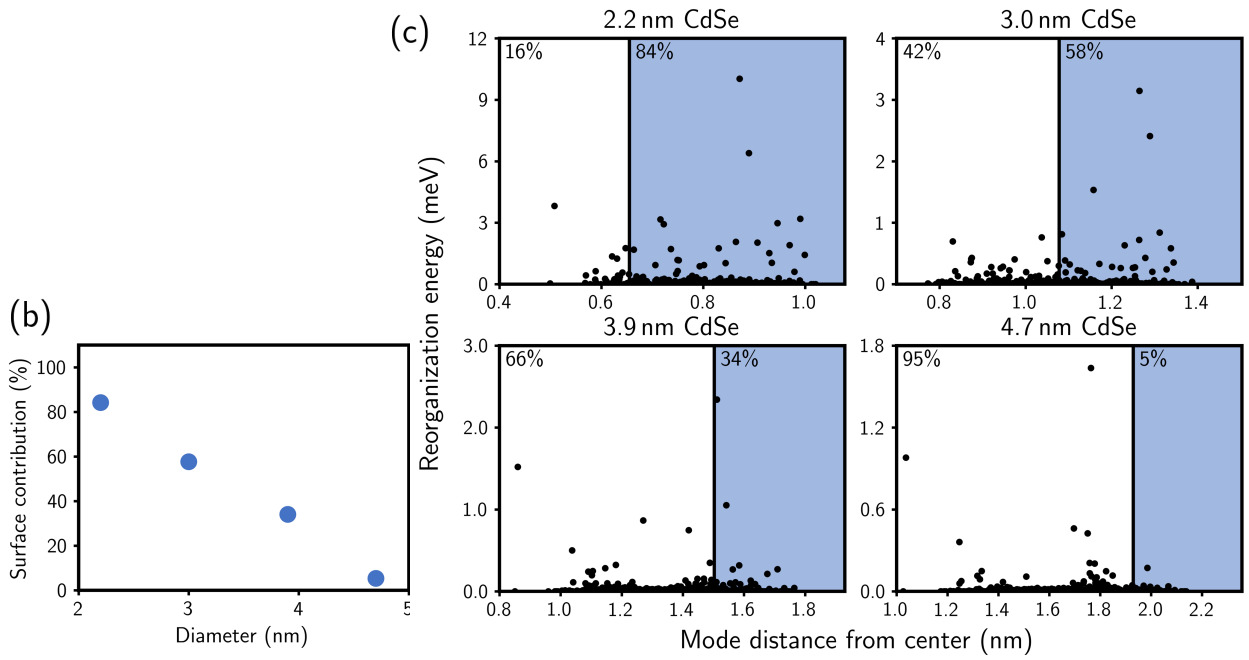

Figure 3: (b) The contribution to the total reorganization energy from modes localized to the surface decreases with increasing NC size. (c) The reorganization energy with phonon mode distance from the NC center for a series of CdSe NCs. Modes in the blue shaded regions are localized to the NC surface. The numbers in the top left of each panel correspond to the percent contributions of the interior (white) and surface (blue) modes to the total reorganization energy.

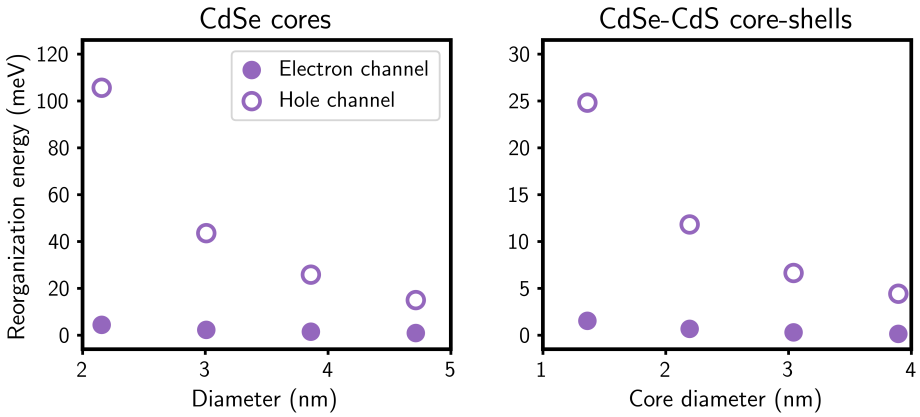

Figure 4: (a) Reorganization energies for CdSe (left) and CdSe-CdS core-shell (right) NCs of various sizes divided into contributions from the electron and hole channels. Reorganization energies for the core-shell NCs are an order of magnitude smaller than those of bare CdSe NCs.

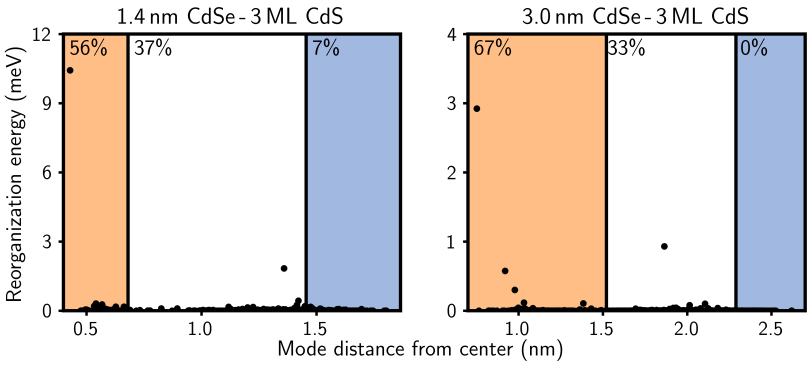

Figure 5: (b) The reorganization energy with phonon mode distance from the NC center for two CdSe-CdS core-shell NCs. Modes in the orange and blue shaded regions are localized to the NC core and surface, respectively. The numbers in the top left of each panel correspond to the percent contributions of the core (orange), shell (white), and surface (blue) modes to the total reorganization energy.

References

(1) Kelley, A. M. Electron-Phonon Coupling in CdSe Nanocrystals from an Atomistic Phonon Model. *ACS Nano* **2011**, *5*, 5254–5262.

(2) Liptay, T. J.; Marshall, L. F.; Rao, P. S.; Ram, R. J.; Bawendi, M. G. Anomalous Stokes Shift in CdSe Nanocrystals. *Phys. Rev. B: Condens. Matter Mater. Phys.* **2007**, *76*, 1–7.

(3) Salvador, M. R.; Graham, M. W.; Scholes, G. D. Exciton-Phonon Coupling and Disorder in the Excited States of CdSe Colloidal Quantum Dots. *J. Chem. Phys.* **2006**, *125*, 184709.